DOI: 10.1002/chem.200600087

Host–Guest Chemistry of Copper(II)–Histidine Complexes Encaged in Zeolite Y

J. Gerbrand Mesu, Tom Visser, Andrew M. Beale, Fouad Soulimani, and Bert M. Weckhuysen*[a]

Abstract: Structural analysis has been carried out on copper(II)–histidine (Cu^{2+}/His) complexes after immobilization in the pore system of the zeolites NaY and de-aluminated NaY (DAY). The aim of this study was to determine the geometrical structure of Cu^{2+}/His complexes after encaging, to obtain insight into both the effect of the zeolite matrix on the molecular structure and redox properties of the immobilized complexes. In addition to N_2 physisorption and X-ray fluorescence (XRF) analyses, a combination of UV/Vis/NIR, ESR, X-ray absorption (EXAFS and XANES), IR, and Raman spectroscopy was used to obtain complementary information on both the first coordination shell of the copper ion and the orientation of the coordinating His ligands. It was demonstrated that two complexes (**A** and **B**) are formed, of which the absolute and relative abundance depends on the Cu^{2+}/His concentration in the ion-exchange solution and on the Si/Al ratio of the zeolite material. In complex **A**, one His ligand coordinates in a tridentate facial-like manner through N_{am}, N_{im}, and O_c, a fourth position being occupied by an oxygen atom from a zeolite Brønsted site. In complex **B**, two His ligands coordinate as bidentate ligands; one histamine-like (N_{am}, N_{im}) and the other one glycine-like (N_{am}, O_c). In particular the geometrical structure of complex **A** differs from the preferred structure of Cu^{2+}/His complexes in aqueous solutions; this fact implies that the zeolite host material actively participates in the coordination and orientation of the guest molecules. The tendency for complex **A** to undergo reduction in inert atmosphere to Cu^{1+} (as revealed by dynamic XANES studies) suggests activation of complex **A** by the interaction with the zeolite material. EXAFS analysis confirms the formation of a distorted four coordinate geometry of complex **A**, suggesting that the combination of zeolite and one His ligand force the Cu^{2+} complex into an activated, entactic state.

Keywords: copper · entactic state · enzyme models · histidine · host–guest chemistry

Introduction

Enzymes reflect, in many respects, the properties of an ideal catalyst. They operate at ambient conditions and combine high activity with an unbeaten enantioselectivity. A disadvantage, however, is their limited thermal stability and chemical resistance. For that reason the development of a more robust catalyst that matches the performance and properties of an enzyme is the ultimate dream of many catalyst researchers. A first step in realizing this dream is obtaining fundamental insight into the chemistry of enzymes. For instance, this can be done by studying a compound that largely resembles (one of) the active sites of an enzyme. Copper ions interacting with histidine (His) moieties are commonly known to play a key-role in many metalloenzymes.[1–6] For this reason Cu^{2+}/His complexes have been studied as model compounds to obtain knowledge on the working mechanism of redox-active enzymes.[7] As a logical next step towards the design of bio-inspired heterogeneous industrial catalysts, Cu^{2+}/His complexes have been incorporated in inorganic hosts, such as zeolites and clay minerals.[7–12] Immobilization of these complexes in the micropores of a zeolite, for instance, provides a structural analogue for the active site of galactose oxidase.[7,9] Besides, the pore structure of the zeolite introduces shape selectivity in the reactions and allows intraparticle transport of reactants and products. Furthermore, the host material supplies additional stability of the incorporated active center, thereby expanding the physical and chemical resistance of the catalyst. The

[a] Dr. J. G. Mesu, Dr. T. Visser, Dr. A. M. Beale, Ing. F. Soulimani, Prof. Dr. Ir. B. M. Weckhuysen
Utrecht University, Inorganic Chemistry and Catalysis
Sorbonnelaan 16, 3584 CA Utrecht (The Netherlands)
Fax: (+31) 30-2511027
E-mail: b.m.weckhuysen@chem.uu.nl

catalytic potential of materials encaged in zeolite Y has already been demonstrated for the epoxidation of alkenes and for the oxidation of alcohols in the presence of *tert*-butyl hydroperoxide at 60 °C.[12]

Structural analysis to determine the coordination geometry of zeolite-encapsulated Cu^{2+}/His complexes has been carried out with a number of different characterization techniques, namely, UV/Vis/NIR spectroscopy,[11,12] X-band electron spin resonance (ESR) spectroscopy,[8,11,12] electron-spin-echo envelope modulation[8,11] (ESEEM) and high-field (W-band) pulsed electron-nuclear double resonance (ENDOR) analysis.[8,11] X-band ESR analysis revealed the presence of two different Cu^{2+}/His species (**A** and **B**) of which the relative amount appeared to be a function of the copper concentration in the ion exchange solution.[11,12] The ^{14}N superhyperfine splitting pattern of complex **B** indicated that nitrogen atoms coordinate to the copper cation;[11] this fact was confirmed by UV/Vis/NIR measurements.[11,12] Complex **A** was concluded to be anchored on the zeolite framework through an oxygen atom as ESEEM showed an intense ^{27}Al modulation. This technique also provided proof for the coordination of an imidazole nitrogen atom in both complexes.[11] From advanced pulsed ESR and ENDOR analysis, complex **B** was initially proposed to have only one His ligand coordinating to Cu^{2+} through two nitrogen atoms, while the other equatorial positions were taken by oxygen atoms from a water molecule and from the support. Later on this proposal was refined to the oxygen atom of a carboxyl group of a second His ligand replacing the coordinating water molecule.[8]

Despite the knowledge of the coordinating geometry of Cu^{2+}/His in the supercage of zeolite Y, the precise effect of the host material on the coordinating preferences of Cu^{2+}/His complexes is still not fully understood. However, knowledge of this effect is essential, as it may influence the catalytic properties of the transition-metal-ion complex after immobilization, particularly since it has been proposed that the enzyme activity originates from the geometric and electronic distortions (caused by the large protein structures) around the metal ion resulting in an "energized state" and enhanced lability.[13] It is therefore reasonable to assume that a combination of multidentate ligands and zeolite structure could induce such geometric strain on the copper species leading to the lowering of the redox potential (a process known as entasis),[13] which could explain the enhanced catalytic activity previously observed. To obtain insight into the host–guest chemistry of the Cu^{2+}/His/zeolite system, we decided to carry out a model study on a series of these solid samples as a logical continuation of the research on the Cu^{2+}/His complexes in aqueous solution as described in two recent papers.[14,15]

It has been shown that X-ray absorption (XAFS), infrared (IR), and Raman spectroscopy can be valuable tools to obtain complementary information not only on the local structure around the central copper ion, but also on the state of protonation of the potential sites for coordination of the His ligand. For that reason we decided to use these techniques in addition to UV/Vis/NIR and ESR spectroscopy to study the structural behavior of Cu^{2+}/His complexes on immobilization in the zeolite pores. Four different Cu^{2+}/His concentrations were used for ion exchange on zeolite NaY to determine the effects of the Cu^{2+}/His loading on the structure of the immobilized complexes and their relative abundance. In addition, two samples of Cu^{2+}/His immobilized on de-aluminated zeolite NaY (DAY) have been prepared to study the influence of the Si/Al ratio of the support. As a result, a better understanding of the host–guest chemistry in this type of bio-inspired heterogeneous catalysts will arise.

Results

N_2 physisorption: The N_2 physisorption isotherms were found to be of the Langmuir type I. Table 1 summarizes the micropore volume of the different Cu^{2+}/His/NaY samples. It decreases from 0.34 $mL\,g^{-1}$ for the sample **a** (with the lowest loading, 0.183 Cu/UC; UC = unit cell) to 0.29 $mL\,g^{-1}$ for the sample **d** with the highest copper loading (0.820 Cu/UC). For the Cu^{2+}/His/DAY samples **e** and **f** no significant decrease in micropore volume was observed with increasing Cu^{2+} loading.

X-ray fluorescence (XRF) analysis: As appears from Figure 1 and Table 1, the copper content in the zeolite material, as determined by XRF spectroscopy, increases proportionally to the Cu^{2+}/His concentration in the ion exchange solution up to a value of 1.5 Cu/UC (0.683 Cu/UC after im-

Table 1. Chemical parameters, results of characterization and ESR simulation data of Cu^{2+}/His loaded zeolite samples.

Sample	[Cu] Ion exchange [Cu/UC]	Si/Al	XRF [Cu] [Cu/UC]	N_2 physisorption micropore volume [$mL\,g^{-1}$]	UV/Vis d–d band maximum [cm^{-1}]	Complex A ESR Rel. abund [%]	$g_\parallel$	$A_\parallel$ [G]	Complex B ESR Rel. abund. [%]	$g_\parallel$	$A_\parallel$ [G]
a	0.25	2.5	0.183	0.34	14500	80			20		
b	0.50	2.5	0.272	0.32	14650	66	2.31	160	34	2.25	180
c	1.50	2.5	0.683	0.32	15000	52			48		
d	4.50	2.5	0.820	0.29	15250	40			60		
e	0.25	100	0.046	0.28	15675	60	2.31	160	40	2.25	180
f	4.50	100	0.112	0.28	16100	30			70		

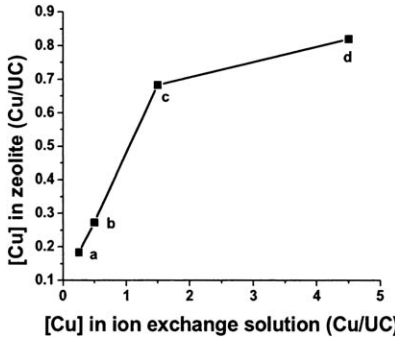

Figure 1. Copper loadings in zeolite NaY as a function of the Cu^{2+} concentration in the ion exchange solution: a) 0.183, b) 0.272, c) 0.683, and d) 0.820 Cu/UC.

mobilization). At a solution concentration of 4.5 Cu/UC, a limit seems to be reached in the number of available sites in the zeolite cages around about 0.8 Cu^{2+} ions per unit cell.

UV/Vis/NIR spectroscopy: The UV/Vis/NIR spectra of the zeolite NaY samples are presented in Figure 2. The spectra display strong absorption bands in the UV part of the spectrum, at 46000 and 36000 cm^{-1} and a weaker one in the visible part of the spectrum at 15000 cm^{-1}. On increasing the Cu^{2+} loading the band at 46000 cm^{-1} remains fixed in position and increases in intensity. Furthermore, the band at 36000 cm^{-1} also gains intensity, but additionally shifts to higher energy (40000 cm^{-1}). The band at 15000 cm^{-1} can be assigned to the Cu^{2+} d–d transition band and is shown in exploded view as an insert in Figure 2. Evidently, the intensity of this band increases with the Cu^{2+} loading as determined by XRF, but it should be noted that this parameter cannot be used straightforwardly for quantification, as the intensity of the d–d transition is also a function of the molecular structure and the geometry of the Cu^{2+}/His complex. The

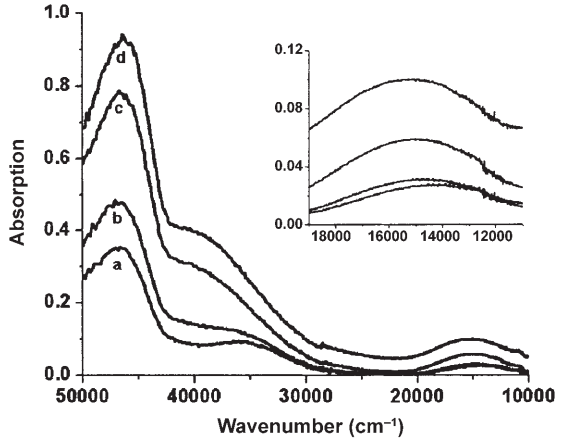

Figure 2. UV/Vis/NIR absorption spectra of Cu^{2+}/His immobilized in zeolite NaY at copper loadings of a) 0.183, b) 0.272, c) 0.683, and d) 0.820 Cu/UC. The insert shows the Cu^{2+} d–d transition band.

position of the d–d transition band shifts from 14500 to 15300 cm^{-1} when the Cu^{2+}/His content in the zeolite increases. A plot of the peak position of the d–d transition versus the Cu^{2+} loading, as shown in Figure 3, reveals that

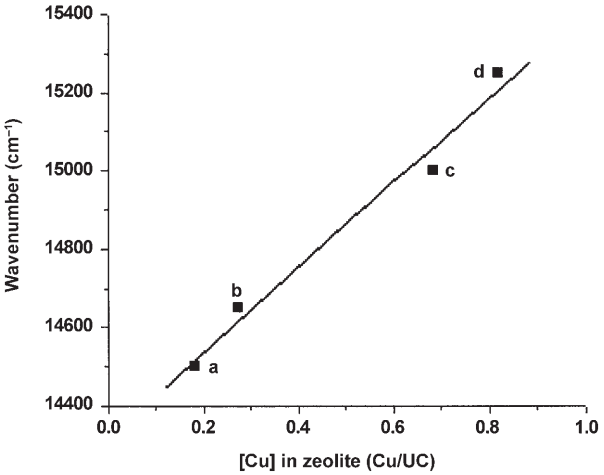

Figure 3. Development of the maximum of the d–d transition band of Cu^{2+}/His/NaY samples **a**–**d** as a function of the Cu^{2+} loading: a) 0.183, b) 0.272, c) 0.683, and d) 0.820 Cu/UC.

the maximum of the d–d transition shifts linearly with the amount of copper present within the zeolite material. This fact points to the presence of at least two different Cu^{2+} species, the ratio of which changes with the Cu^{2+} loading. Finally, it should be noted that the precise position of the d–d transition band is sensitive to the state of hydration of the zeolite matrix. Upon drying in a desiccator, a red-shift of the band was observed, whereas rehydration of the samples resulted in a shift to the original position.

ESR analysis: The first derivatives of the X-band CW-ESR absorption spectra of the Cu^{2+}/His/NaY samples are shown in Figure 4 (top). It is evident from the spectra that free Cu^{2+} is absent, since a species with the ESR parameters for Cu^{2+} on zeolite Y ($g_{\|}=2.39$, $A_{\|}=129$) is not observed. Thus all copper is coordinated to His. The spectra reveal the contribution of two distinct ESR sub-spectra, which implies that at least two different Cu^{2+}/His complexes, **A** and **B**, must be present in the zeolite support. The absolute abundances of the two complexes was determined from the ESR spectra and the results are presented in Figure 5, expressing the ESR intensity as a function of the Cu^{2+} loading in the zeolite. Evidently, the total number of complexes (**A**+**B**) increases with the Cu^{2+} concentration, but it is apparent that the ratio **A**/**B** changes too. At low loadings complex **A** is the major species, whereas complex **B** becomes dominant at a high copper content. The optimized values for both complexes are presented in Table 1; complex **A** has a higher $g_{\|}$ and lower $A_{\|}$ value than complex **B**. The same complexes **A** and **B** were also found to be present in the Cu^{2+}/His/DAY samples. The corresponding ESR parameters and the calcu-

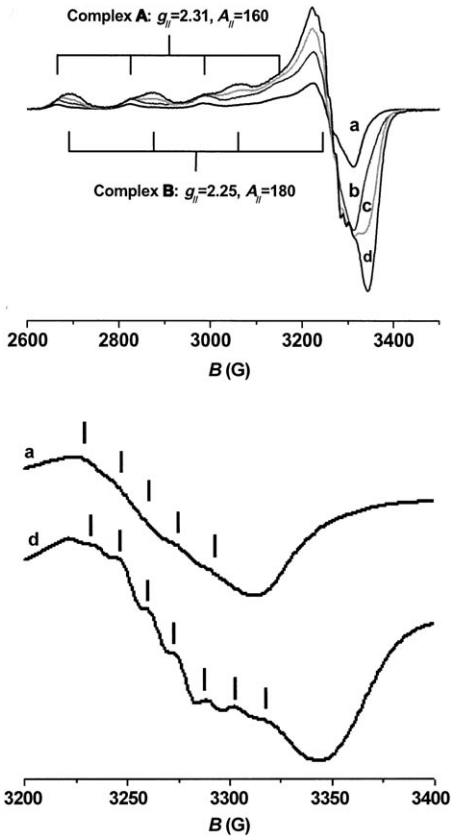

Figure 4. Top: First derivative CW-ESR spectra of Cu^{2+}/His immobilized in zeolite NaY at different copper loadings: a) 0.183, b) 0.272, c) 0.683, and d) 0.820 Cu/UC. Bottom: The hyperfine splitting patterns of sample **a** (0.183 Cu/UC) and sample **d** (0.820 Cu/UC).

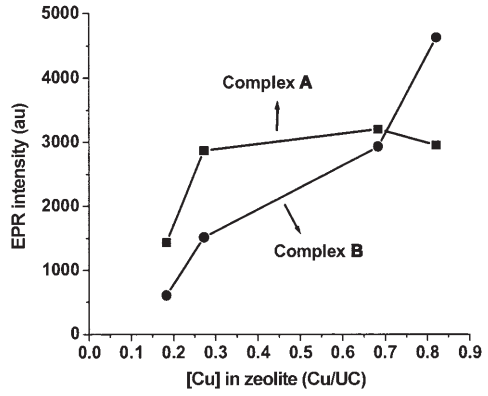

Figure 5. The absolute distribution of complex **A** (■) and complex **B** (●) in Cu^{2+}/His/NaY (based on ESR results) as a function of the copper concentration in the zeolite, as determined by XRF analysis.

lated relative abundance of the two complexes of all samples are summarized in Table 1.

The exact number of nitrogen atoms in the first coordination sphere around the Cu^{2+} ion was established for each of the samples **a**–**f** by investigating the splitting pattern in the hyperfine region of the overall ESR spectra (Figure 4 bottom). For sample **a**, a five fold hyperfine splitting pattern is observed, which points to the presence of two N-atoms in the vicinity of the Cu^{2+} cation. In contrast, for sample **d**, a sevenfold splitting pattern is established, which proves the presence of three N-atoms in the first coordination sphere. The same seven-fold splitting pattern was observed in the spectrum of the Cu^{2+}/His/DAY sample **f**. The copper concentration in sample **e** was too low to extract reliable conclusions.

EXAFS analysis: The results of the 1st shell analysis of the k^3-weighted EXAFS spectra for the Cu^{2+}/His/NaY samples data recorded at room temperature in air are summarized in Table 2 and the corresponding Fourier transforms are shown

Table 2. Parameters derived from an analysis of k^3-weighted EXAFS data.[a]

Sample	r [Å]	CN	Ligand	σ^2 [Å^2]	E_f [eV]	R factor
a	1.97	2.7	N	0.012	−7.79	35.86
a (2nd shell)	2.32	0.8	O	0.018		
b	1.97	3.2	O	0.012	−6.64	33.24
c	1.96	3.5	O	0.010	−3.67	35.41
d	1.95	3.8	N	0.010	2.81	29.71

[a] r = Average 1st shell distance, CN = coordination number, E_f = edge position (fermi energy), σ^2 = Debye–Waller Factor.

in Figure 6. In particular two trends can be clearly observed. The first is related to the average first Cu nearest neighbor distance, which tended to reduce with increased copper loadings. However, since these changes are within the standard error limits for the technique (±0.02 Å) these distances can be regarded as being very similar for all samples. The second trend is related to differences in the coordination numbers, which implied that structural differences in the local Cu environment existed. Significantly, as the results in Table 2 and Figure 6 showed, the coordination number appeared to increase with increasing Cu loadings in the zeolite ranging from about three (best fit obtained with a shell of oxygen atoms) for sample **a** to approximately four (best fit obtained with a shell of nitrogen atoms) for sample **d**. These

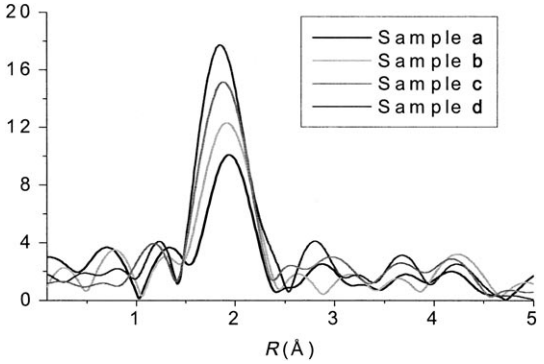

Figure 6. Fourier transform data for the EXAFS spectra of Cu^{2+}/His immobilized in zeolite NaY at different copper loadings: a) 0.183, b) 0.272, c) 0.683, and d) 0.820 Cu/UC. Both the real part and the envelope are presented.

observations therefore followed the trend observed in the EPR data, in which more of complex **B** was observed to form within the zeolite and hence also explains why a better fit was obtained when fitting the data using a shell of nitrogen atoms. However this also suggested that the samples dominated by complex **A** at low loading possessed an unusually "undercoordinated" copper environment. Further attempts at fitting this data allowed us to identify an additional Cu–O ligand (shown in Figure 7) at a distance of 2.32 Å suggesting a distortion of the copper environment, but still maintaining the four-coordinate state.

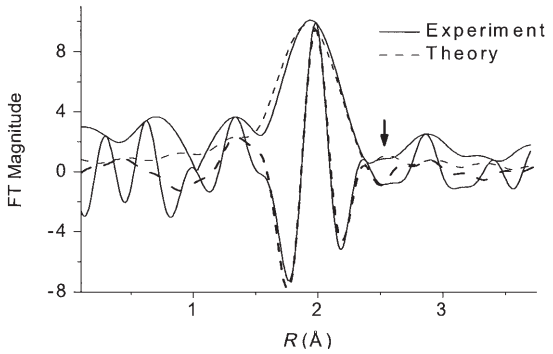

Figure 7. Real and imaginary parts of the Fourier transform from the fitted EXAFS spectra for sample **a**. The arrow indicates the location of the long Cu–O bond at 2.32 Å.

XANES analysis: Additional, corroborative information was obtained from the normalized XANES spectra shown in Figure 8. The arrows labeled X and Y point towards the most significant differences between the two spectra. These correspond to features at approximately 8986 and 8990–9000 eV, respectively, which are present in sample **d**, but not (or in the case of feature Y at a lower intensity) in **a**. The origin of these features is not clear, but is certainly associated with a 1s–4n ($l=0$ or 1; $l=$quantum number) quadrupole and/or dipole transitions.[17–19] Interestingly the intensity of the transition marked X has shown some dependency on the local structure around the absorber, mainly related to the tendency of axial ligands to undergo a tetragonal (Jahn–Teller) distortion.[17,20] Indeed it has been proposed that both the degree of axial distortion and the number of axial ligands produce such effects. However, such conclusions have been drawn based upon only a limited number of studies and so it is difficult to draw strong conclusions about the copper environment from the structure of the XANES. However, the lack of a feature at about 8986 eV does suggest that the sample does not possess strongly displaced axial ligand(s) (at least not greater than 0.4 Å away from the equatorial ones). In comparison changes in the area marked Y are not so well characterized, especially since multiple scattering and multiple electronic excitation effects often complicate this region. However a recent paper by Chaboy et al. was able to simulate multiple electronic excitations using two final state configurations $3d^9$ and $3d^{10}L$ (in which L denotes a hole from the ligand).[21] Although these transitions are not so clearly resolved here it is possible to suggest that the much weaker transition intensity (especially the $3d^{10}$ L transition) seen in sample **a** could be explained by the lower coordination number and/or oxygen ligands around the copper in this sample.

When the same Cu^{2+}/His/NaY samples were studied in He at 77 K, it was observed that a feature at 8983 eV evolved and increased in intensity with the exposure time to the X-ray beam. This is illustrated in Figure 9 by the spectra of sample **a**, obtained at three different stages in time. As reported recently,[22] the appearance of this pre-edge feature can be assigned to the reduction of Cu^{2+} to Cu^{1+}. Under influence of the X-ray beam, radiolysis of the water (present in the micropores of the zeolite material) occurs. Amongst

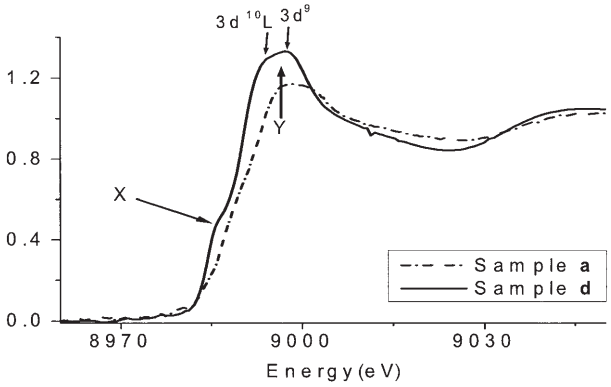

Figure 8. Normalized XANES spectra recorded for samples **a** and **d**. A feature at about 8988 eV is highlighted by the arrow marked X,and another at the center of the peak between 8990 and 9000 eV is marked with an arrow labeled Y. The position of the two excitations and their final state configurations for sample **d** are highlighted. The spectrum of sample **a** was recorded at beamline X1.1 (Hasylab), the spectrum of sample **d** at BM29 (ESRF). Both spectra were collected in 45 min in air at room temperature.

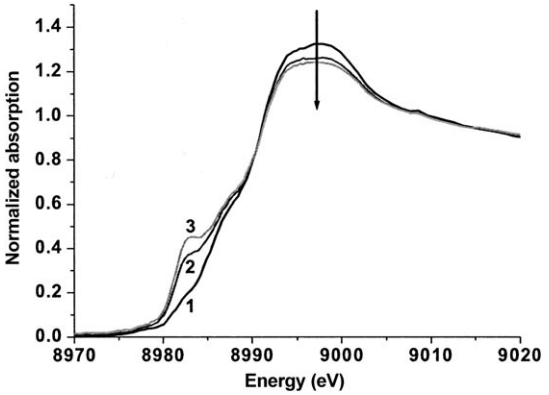

Figure 9. Development of the X-ray absorption near-edge structure of the Cu^{2+}/His/NaY sample containing the lowest copper concentration (sample **a**) over time. The spectra are labeled according to the time of exposure to the X-ray beam: 1 = shortest, 3 = longest. The arrow also indicates increasing time of exposure. The absorption intensity increases with respect to time at the position of the numbers 1–3, but decreases with respect to time at the position of the arrow.

others, hydrated electrons are generated that can reduce the copper within the zeolite samples. The observed phenomenon is most prominent in the low Cu^{2+}-loaded samples **a** and **b**. To gain insight into the origin of this effect the normalized intensity of the Cu^{1+} feature at 8983 eV has been plotted as a function of the X-ray exposure time for all samples (Figure 10). Indeed, the reduction process proceeds fastest

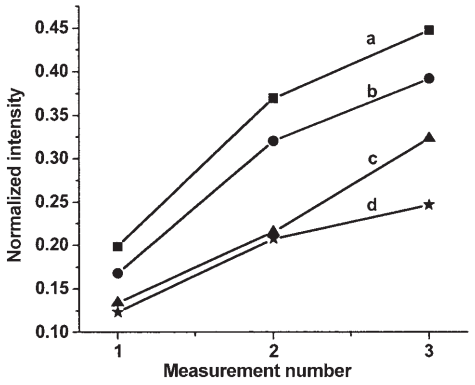

Figure 10. Effect of the X-ray exposure time on the development of the Cu^{1+} pre-edge feature at 8983 eV in the normalized X-ray absorption spectra of the Cu^{2+}/His/NaY samples at different copper loadings: a) 0.183, b) 0.272, c) 0.683, and d) 0.820 Cu/UC. From this figure it can be concluded that the normalized intensity is proportional to the relative amount of complex **A** within the zeolite material (cf. XRF results in Table 1).

for the sample with the lowest Cu^{2+}/His loading (and thus with the highest relative amount of complex **A**). When corrected for the relative amount of complex **A** present in the sample (by dividing the intensity of the pre-edge feature by the relative amount of complex **A**, as determined by ESR, see Table 1) and for the average beam current during the individual scans, the four lines coincide. This indicates that the reducing effect of the X-ray beam is only affecting complex **A** (which is the major constituent of sample **a**), leaving complex **B** (which is the prevailing structure in sample **d**) unaffected. The appearance of the feature at 8983 eV was only observed for the Cu^{2+}/His/Y samples that were studied in a controlled He atmosphere. For the samples measured in air the feature was not observed, as back-oxidation under influence of oxygen probably occurs.

Vibrational spectroscopy: The IR spectra of the Cu^{2+}/His/NaY samples and the His/NaY samples are dominated by the strong absorption characteristics of the NaY support material. After subtraction of the spectrum of the bare NaY material the difference spectra of the samples **a** and **b** were too weak to be useful for interpretation. A better signal to noise ratio was obtained particularly for sample **d** with the highest Cu^{2+}/His concentration, but this spectrum appeared to be virtually identical to that of the reference compound His/Y. To illustrate this, the spectrum of sample **d** is presented in Figure 11, together with the spectra of the reference compound His/NaY and His in aqueous solution recorded at

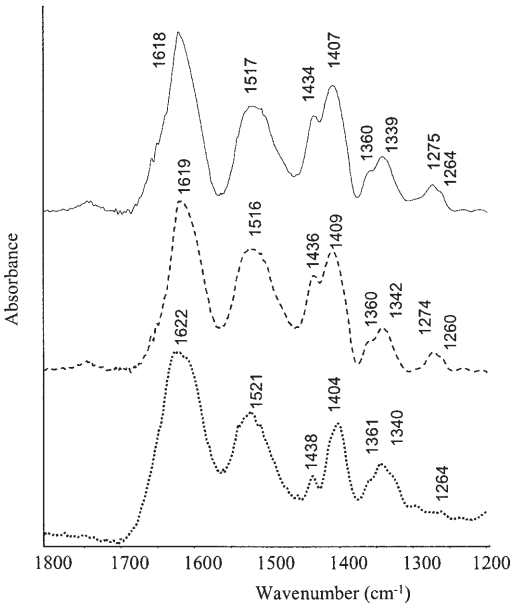

Figure 11. IR spectra of Cu^{2+}/His/NaY at copper loadings of 0.820 Cu/UC (top), His/NaY (middle), and His in aqueous solution at pH 5 (bottom).

pH 5 (for the assignments of the bands we refer to earlier work[14,15]). Because of interfering bands of the zeolite support only the range 1800–1200 cm^{-1} is shown. The same procedure was followed for the Cu^{2+}/His/DAY compounds, but interpretable spectra were not obtained because of the too low Cu^{2+}/His concentrations in these samples. As with the IR spectra, useful Raman spectra were only obtained for the high concentrated sample **d** after subtraction of the spectrum of pure zeolite NaY. Apart from small differences in peak intensity, the Raman spectrum is virtually the same as that of the difference spectrum of the His/NaY reference material. Moreover, as was the case for IR spectra, the Raman spectrum largely resembles that of His in aqueous solution recorded at pH 5.[14]

Discussion

Effects of the zeolite host: As already mentioned, the IR and Raman spectra of the Cu^{2+}/His/NaY samples **c** and **d** are very similar to the ones of the reference compound in which only free His was ion exchanged onto the support. This is not surprising regarding the excess of His in the solutions that was used to prepare the samples. Referring to literature, it can be calculated that 80% of the His molecules are not complexed to Cu^{2+} complexes, but are ion exchanged on the support.[6] Consequently, the IR and Raman spectra represent mainly these non-complexed His species. However, as we reported recently,[14,15] IR and Raman can be used to determine the state of protonation of the His molecules. This is dependent on the "pH" of the local environment and thus, the vibrational spectra of **c** and **d** can be used as an indirect tool to establish the "pH" within the zeo-

lite matrix. Therefore, we compared the IR and Raman spectra of samples **c** and **d** with the data of His in aqueous solutions at different pH's, although it should be noted that the spectra are not fully comparable, as the environment in the zeolite is not fully aqueous. Referring to our recent paper on this subject,[14] the strong IR band at 1517 cm^{-1} (Figure 11) proves that the primary amino group (N_{am}) is protonated, while the absence of a C=O stretching band around 1735 cm^{-1} shows that the carboxyl group is the only site that is deprotonated. The pK_a values of the two groups were found to be 9.1 and 1.8, respectively, and it follows that the pH must be between these two values. Furthermore, the strong bands at 1485, 1264, 1185, and 991 cm^{-1} in the corresponding Raman spectrum can be attributed to the fully protonated form of the imidazole ring, which implies that this structural element is not involved in the bonding of His to the support either. The pK_a value of this group is 6.0 and so, the "pH" inside the zeolite must be below pH 6. Closer examination of the spectral fingerprints reveals a striking similarity with the spectra of free His obtained at pH 5, which is well illustrated by the IR spectra in Figure 11. Hence, it can be concluded that the acidity inside the zeolite corresponds to a "pH" of about 5. At this pH, His is mainly present in the ionic state $[H_3His]^+$ and with this in mind, it is easy to conclude that ion exchange of Na^+ with $[H_3His]^+$ largely occurred during the preparation of the samples.

Information on the chemical state of the host matrix can also be derived from the UV/Vis/NIR spectra. Comparison of the spectra of the Cu^{2+}/His complexes immobilized in the zeolites with the ones recorded in aqueous solution shows a difference in the position of the Cu^{2+} d–d transition band of about 1600 cm^{-1}. In theory, the position of the band depends on the nature of the chelating atoms and their distance towards the central copper cation, but it is evident that the matrix, that is, the solvent or the support, affects this parameter. Apparently, the effect of the zeolite support on the Cu^{2+} complex is a red shift of the d–d transition band. It also explains the difference in peak position that we observed in the UV/Vis/NIR spectra before and after thorough drying of the Cu^{2+}/His/NaY samples. Since a zeolite matrix can adopt different states of hydration, it implies that it is, in principle, possible to change the properties of the guest complex (Cu^{2+}/His) by adjusting the state of hydration of the host material.

Another important effect of the support on the complexes can be derived from the XAFS results. As we already noted, for the samples that were measured in a He atmosphere, the reduction of Cu^{2+} upon exposure to the synchrotron beam is the largest for the samples with low Cu^{2+} loadings, that is, the samples with relatively the highest amount of complex **A**. Normalizing the data for the relative abundance of complex **A** (by and for the beam current) reveals that the reduction process proceeds in the same way for all samples; this result indicates that only complex **A** is susceptible to the influence of the X-ray beam. So the zeolite host material affects the chemistry of the guest complex by making complex **A** more susceptible towards reduction than complex **B**. There are different possible explanations for this behavior. The zeolite increases the redox potential of complex **A** with respect to complex **B**, thus facilitating reduction of the Cu^{2+} ion by the free electrons (with a reduction potential of −2.9 V vs. SHE) that are generated by the radiolysis of water in the pores of the zeolite material. It is commonly known that the redox potential of metal ions increases with the electronegativity of the ligands. There are more oxygen atoms (with a higher electronegativity) in the first coordination sphere around Cu^{2+} in complex **A** than in species **B**. An alternative and yet more intriguing possibility is that the combination of the His ligand and zeolite at low loadings forces the Cu^{2+} into a entactic state thus making its reduction to Cu^{1+} much more facile. This phenomenon was expressed by the tendency of Cu^{2+} to adopt the preferred trigonal geometry of Cu^{1+} despite the interatomic distances of Cu to the surrounding O and N atoms remaining similar. In principle, reduction of Cu^{2+} towards Cu^{1+} should be attended with a drop in the average bond lengths, but this was not observed. Either way the ease of reduction of complex **A** appears to explain the observed activity trend in the catalysis experiments with the Cu^{2+}/His systems encaged in zeolites in literature.[7,12] Higher turnover frequency (TOF) numbers were obtained for the oxidation reaction in the systems with the highest relative amount of complex **A** and although pore-blocking at higher Cu^{2+}/His loadings will result in a lower TOF, it is evident that the TOF will increase when it is easier for Cu^{2+} to be reduced in the catalytic cycle. The fact that when the XAS measurements are performed on the same samples in air, no reduction of the copper was observed indicates that complex **A** has a conformation that makes the complex very sensitive towards back-oxidation by molecular oxygen. It is important to note that catalytic activity in oxidation reactions with the immobilized Cu^{2+}/His complexes only was observed when peroxides were used as oxidant. No activity was observed when molecular oxygen was used as oxidant.[7,12]

Molecular structure of the zeolite encapsulated complexes: Structural information on the Cu^{2+}/His complexes that are encaged in the zeolite pores is primarily extracted from the UV/Vis, ESR, and EXAFS-spectra. All techniques show changes in the spectral data upon increasing the Cu^{2+}/His concentration of the ion-exchange solution. This implies that the coordination around the central Cu^{2+} ion changes and hence more than one type of Cu^{2+}/His complex is immobilized. As shown in Figures 4 and 5, the ESR spectra clearly reveal the presence of two Cu^{2+}/His complexes, **A** and **B**, of which **A** is the dominant one at low Cu^{2+}/His concentrations and **B** the major species with high Cu^{2+}/His concentrations. Furthermore, the hyperfine splitting patterns point to two nitrogen atoms in the first coordination sphere in complex **A** and three in complex **B**. These observations are identical to the results of Baute et al.[8] who proposed the molecular structures for both complexes to be as shown in Figure 12.

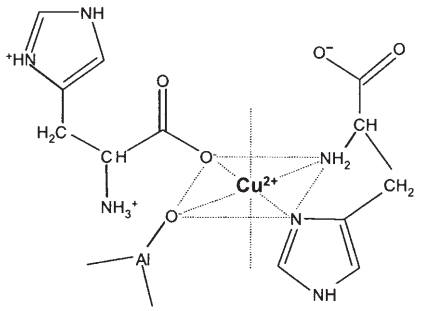

A

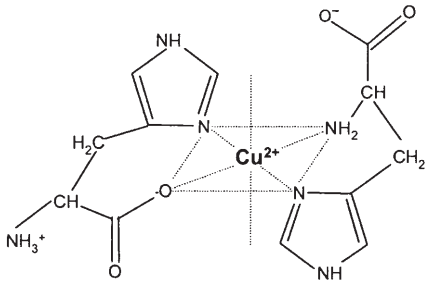

B

Figure 12. Structures of the two Cu^{2+}/His complexes **A** and **B** immobilized in zeolite Y, as proposed by Baute et al.[8]

In line with these results, the interpretation of our UV/Vis/NIR data confirms the larger number of coordinating nitrogen atoms on increasing the Cu^{2+}/His concentration. Figure 2 shows that the d–d transition band shifts to higher energy on going from sample **a** to **d**, that is, from mainly complex **A** to mainly complex **B**. As EXAFS analysis reveals that the distance of the atoms in the first coordination sphere around the Cu^{2+} ion is similar for all samples, this shift must be due to a larger ligand field splitting between the d orbitals of the Cu^{2+} complex and this can only be attributed to an increase in the amount of nitrogen atoms coordinating to the Cu^{2+} ion.

The UV/Vis/NIR, ESR and EXAFS results of the Cu^{2+}/His/DAY samples **e** and **f** confirm the observation by Grommen et al.,[11] that the formation of complex **A** is related to the presence of aluminum in the zeolite matrix. The ESR parameters are identical to the values of the Cu^{2+}/His/NaY samples (see Table 1) and in sample **e**, complex **A** is the dominating species. However, despite the very low Cu^{2+}/His concentration that was used to prepare sample **f**, complex **B** has become the major component due to the lack of aluminum atoms in the framework of the supporting zeolite material. Note that the Cu^{2+} concentration in this sample is even lower than that in the Cu^{2+}/His/NaY sample **a** in which complex **A** is the most abundant structure. It implies that the relative amount of the guest species **A** and **B** can be tuned by changing the aluminum content of the zeolite host material.

Additional structural information on the complexes can be derived from the UV/Vis/NIR spectrum, as coordination of an imidazole group to Cu^{2+} is known to give rise to a characteristic band pattern.[23–27] The absorption originates from ligand-to-metal charge-transfer (LMCT) transitions of the higher lying orbitals of the imidazole ring to the Cu^{2+} cation. Next to a σ lone pair, there are two filled π-type orbitals on the imidazole ring that are high in energy[27] and as a consequence, three LMCT transitions can occur from these orbitals to the empty $\sigma^*(x^2-y^2)$ orbital on the Cu^{2+} ion. The transition from the lone pair is the highest in energy and the intensity is independent of the orientation of the imidazole ring with respect to the Cu^{2+} ion.[23] This LMCT transition is known to absorb around 46000 cm^{-1} and indeed, a band at this position is present in the spectra of all samples (Figure 2). It follows that at least one imidazole group coordinates to Cu^{2+} in both complexes **A** and **B**. The two other LMCT transitions are lower in energy[27] and the position and intensity of the corresponding bands are less defined, as they are sensitive to the position of the ring with respect to the central metal ion.[23] These transitions can be easily assigned to the bands at 40000 cm^{-1} and 36000 cm^{-1}, respectively. However, the band at 36000 cm^{-1} is the strongest for the low loaded sample **a**, whereas the band at 40000 cm^{-1} is the most intense for the high loaded sample **d**. This confirms not only the presence of two different complexes, **A** and **B**, but also implicitly proves that the structure of both complexes differ in the orientation of at least one of the two His ligands towards Cu^{2+} through the imidazole ring. From these results, we conclude that the coordination around Cu^{2+} is NNOO in complex **A** and NNNO in complex **B**, which is in accordance with the results of Baute et al.[3] and Grommen et al.[11] However, the results of our multitechnique study suggest that the conclusions presented previously for the two complexes can be fine-tuned further. From the EXAFS data for complex **A**, we were able to determine a two shell model consisting of three short Cu–N/O distances (≈1.97 Å) and one long Cu–O distance (≈2.32 Å). From previous data on copper-based amino acid complexes, it has been observed that such long Cu–O type bonds are normally typical for axially coordinating ligands in octahedral complexes. In view of these observations we propose that the structure of the Cu^{2+}/His/NaY complex **A** can be rationalized as a complex consisting of only one His ligand exhibiting a tridentate facial coordina-

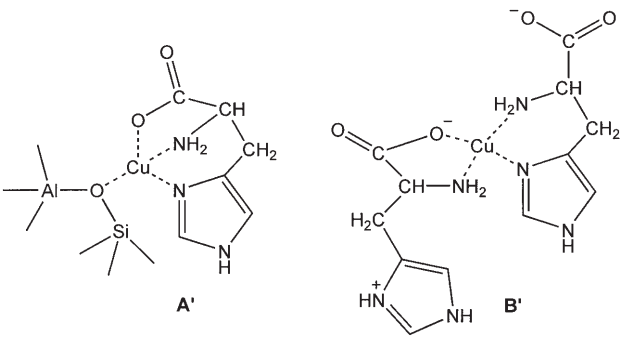

Figure 13. Proposed refined structures of Cu^{2+}/His complexes **A′** and **B′** immobilized in zeolite Y.

tion (Figure 13, complex **A′**) with the remaining oxygen ligand from the first coordination sphere being contributed by a zeolite oxygen. The relatively large Cu–O distance (≈2.32 Å) might be due to sterical hindrance between the zeolite structure and the facial coordinating His ligand. For complex **B**, Baute et al. and Grommen et al. proposed coordination of both His ligands through N_{im} based of results from ESEEM-measurements, but based on our results it can be argued that this structure proposal is not fully correct. Firstly, as follows from the IR and Raman spectra, the "pH" inside the zeolite is around 5 and as we recently demonstrated, a bisglycine-like NONO coordination and a combined glycine/histamine-like NNNO chelation is much more likely under these circumstances (Figure 13, complex **B′**).[15] Secondly, the corresponding seven-membered ring coordination (N_{im}, O_c) may not very stable as it is associated with a considerable ring tension regarding the N···O distance in this structure. This should affect the EXAFS data in a similar way to that we observed for the Cu^{2+}/His complexes in aqueous solution.[15] However, the EXAFS data are similar and for that reason we propose the structures **A** and **B**, presented in Figure 13 as refined modifications of the complexes proposed by Baute et al.[8] and Grommen et al.[11]

Complex formation: Based on the preceding results, we have developed the following mechanism for the formation of the Cu^{2+}/His complexes **A** and **B**. The pH in the ion-exchange solution is kept at 7.3, which implies that in the aqueous phase Cu^{2+} will be mainly present as a complex with two His ligands that coordinate through the nitrogen atoms (NNNN).[15] The charge of this complex is neutral, whereas the excess of free His ligands are charged partly neutral (H_2His^0) and partly positive (H_3His^+). On entering the pores of the zeolite, first the H_3His^+ ions will exchange with protons and sodium atoms in the zeolite framework, thus compensating for the charge deficiency on the aluminum atoms in the zeolite framework. This process is attended with a decrease of the pH inside the pores of the zeolite to about 5. As a result, not only H_2His^0 will become protonated to H_3His^+, but also the NNNN coordination of the Cu^{2+}/His will convert to the histamine/glycine-like coordinated NNNO complex, while the total charge of the Cu^{2+}/His becomes 1^+ from neutral. Consequently, this opens the possibility for the complex to exchange sodium atoms as well, resulting in anchoring on the zeolite support either through Cu^{2+} (complex **A**) or the positively charged imidazole ring (complex **B**). It should be noted that the amount of H_3His^+ ions within the pores is rapidly increasing too, which means that the ion-exchanging process with the available Brønsted sites will be a competition between the free NNNO-coordinated Cu^{2+}/His complex and the excess of H_3His^+ ions. Evidently, the latter will take the majority of the available places.

Regarding the effect of the Si/Al ratio on the relative abundance of **A** and **B** and the fact that the absolute amount of complex **A** is stabilizing at higher ion-exchange concentrations, it can be concluded that complex **A** is favored over **B**. However, its formation is hampered by the limited number of available sites in the near vicinity of an aluminum atom. It follows that a position in the middle of the supercage is the only possibility left, in case the aluminum atoms in the outer cages are occupied. This hypothesis also explains why no copper–aluminum interaction is found in the ESEEM measurements for complex **B**.[8,11] Another option for a possible position is one between two neighboring supercages, but this is rejected for the same reason.

Conclusions

The combined use of UV/Vis/NIR, ESR, and X-ray absorption analysis has proven to be a powerful method to obtain complementary information on the molecular structure of Cu^{2+}/His complexes immobilized in the cage of the zeolite supports NaY and DAY. Two complexes (**A** and **B**) can be formed in the micropore system of the zeolite material, depending on the copper concentration used in the ion-exchange procedure and the aluminum content of the zeolite support material. The geometrical structure of the complexes differs from the ones that are present in the aqueous ion-exchange solution at pH 7.3. In complex **A**, one His molecule coordinates to Cu^{2+} in a tridentate facial manner. The remaining equatorial position anchors the complex on the support through an oxygen atom that is connected to an aluminum atom in the framework. In complex **B**, one His ligand coordinates in a glycine-like coordination (N_{am},O_c), but the other one takes a histamine-like chelation (N_{am},N_{im}). This complex is trapped in the supercage through the positive charge on the non-coordinating imidazole ring. IR and Raman spectroscopy are not sensitive enough to obtain structural information on the complexes, but the spectra revealed an increased acidity within the zeolite pores corresponding to a pH of 5. It explains why the geometrical structure of complex **B** matches with the preferred structure of the Cu^{2+}/His complex in aqueous solution at this pH. On the other hand, complex **A** differs from this structure, which implies that zeolite host materials are able to affect the coordination and orientation of the guest molecules. Besides, it illustrates that zeolites are not just inorganic supports that can be used for site isolation and shape selectivity, but that they actively participate in the coordination chemistry and geometry of the guest complex. Vice versa, they affect the chemistry of the guest complexes by imposing a different chemical environment than in, for example, aqueous solution. This mutual interaction is illustrated by the enhanced reducibility of the Cu^{2+}/His complex **A** on exposure to X-ray radiation, while complex **B**, which has a counter part in aqueous solution, is not reduced. The trend from Cu^{2+} towards Cu^{1+} in complex **A** is probably due to a distortion of the square pyramidal geometry of Cu^{2+} towards the favored trigonal structure of Cu^{1+}. The result is an energized or entactic state—a similar state to that seen for active copper species in many enzymes.[13] These results demonstrate that the immobilization of transition-metal-ion complexes in in-

organic support materials may open new perspectives in the design of new catalyst materials with novel applications.

Experimental Section

Sample preparation: Two commercially available zeolite support materials were ion-exchanged with a copper–histidine complex (Cu^{2+}/His): NaY zeolite (AKZO Nobel, Si/Al ratio of 2.5, surface area of 900 $m^2 g^{-1}$and pore volume of 0.34 mL g)$^{-1}$ and DAY zeolite (Wessalith, Si/Al ratio of 100, surface area of 700 $m^2 g^{-1}$and pore volume of 0.29 mL g)$^{-1}$. The DAY material is a Y-type zeolite with a faujasite structure with a very high Si/Al ratio. The zeolite was prepared by means of a special $SiCl_4$ treatment that yields zeolite Y structure in which almost all of the aluminum sites are occupied by silicon. However, the properties of the lattice framework are fully maintained, whereas medium sized pores and defects are absent. Prior to ion exchange with Cu^{2+}/His the zeolites were put in the Na^+ form by two successive ion exchanges with NaCl solutions (1 M), washed Cl^- free and dried in air at room temperature overnight.

The NaY zeolite was exposed to solutions of Cu^{2+}/His (1:5) in aqueous solutions at Cu^{2+} concentrations of 6.5×10^{-5} M, 1.3×10^{-4} M, 3.9×10^{-4} M and 1.2×10^{-3} M, which corresponds to respectively 0.25, 0.5, 1.5 and 4.5 copper atoms per unit cell (Cu/UC) of the zeolite Y material present in the ion-exchange solution. For DAY, concentrations corresponding to 0.25 and 4.50 Cu/UC were applied. First, equilibration of NaY (5 g) in of demineralized water (1 L) was performed for 3 h at pH 7.3. The pH was adjusted by using solutions of NaOH (0.1 M) and/or HNO_3 (0.1 M). Next, the aqueous solution of $Cu(NO_3)_2{\cdot}3H_2O$ (Merck, p.a.) and L-histidine (Acros Organics) in a 1:5 ratio at pH 7.3 was added and the mixture was stirred for 48 h at room temperature. The pH of the solution was kept constant at pH 7.3 by adding NaOH or HNO_3 when necessary. In the following step, the exchanged loaded zeolite material was isolated by vacuum filtration, washed three times with demineralized water and dried (333 K, 24 h). The same procedure, only without the addition of $Cu(NO_3)_2{\cdot}3H_2O$, was followed to obtain His/NaY and His/DAY as a reference material. Additional ion exchange experiments were carried out to determine the effect of the ion exchange time on the amount of Cu^{2+} complexes exchanged on the zeolite material, but no significant increase was observed for longer exchange times.

Characterization: Prior to spectroscopic characterization, nitrogen physisorption experiments were carried out to determine changes in the zeolite pore volume as result of ion exchange with Cu^{2+}/His. After degassing of the solid samples for 24 h at 373 K in vacuum, the analysis was performed at 77 K with a Micromeritics ASAP 2400 apparatus. Next, the micropore volumes and pore size distributions were determined with standard BET and BJH theory.

X-ray fluorescence (XRF) analysis was carried out to establish the exact copper contents of the solid samples after immobilization of Cu^{2+}/His. Measurements were performed on a Spectro X-lab 2000 instrument. The calculation of the copper concentration in copper atoms per unit cell (Cu/UC) was based on the amount of aluminum and silicon present in the same sample and assuming that one unit cell of the zeolite material consists of 192 Si and Al tetrahedra.

UV/Vis/NIR measurements were carried out in diffuse reflectance with a Cary-500 spectrophotometer (Varian), equipped with an integrating sphere. Bare NaY zeolite powder was used as a white background. Spectra were recorded from in the range 50000 to 10000 cm^{-1}.

X-band ESR spectra were recorded on a Bruker ESP300E spectrometer at Leuven University (Belgium). The instrument was operated near 9.5 GHz and was equipped with a Bruker ER4103TM cavity. The samples were recorded at a temperature of 120 K in a quartz tube. Data acquisition and spectral manipulation were performed by using the instrument software. Spectral simulation was carried out by using the commercially available Symphonia software. The shape of each sub-spectrum was chosen as a molecule with an axial Zeeman interaction plus an axial hyperfine interaction to the copper nucleus ($I=3/2$). The experimental accuracy did not require simulation as a mixture of $^{63}Cu/^{65}Cu$ isotopes.

X-ray absorption measurements on the Cu^{2+}/His/NaY samples with the lowest copper concentrations (samples **a** and **b**, Table 1) were collected in air at room temperature in the fluorescence mode at wiggler station X1.1 of Hasylab (Hamburg, Germany) by using a Si(111) double crystal monochromator. The monochromator was detuned to 50% of the maximum intensity to avoid higher harmonics in the X-ray beam. The Cu^{2+}/His/NaY samples with the high copper concentrations (samples **c** and **d** in Table 1) were measured in air at room temperature in transmission at beamline BM29 of the ESRF (Grenoble, France), with a Si(111) double crystal monochromator. Higher harmonic rejection was performed by detuning both monochromator crystals by 50%. Additional X-ray absorption spectra of all Cu^{2+}/His/NaY samples were collected at beamline BM26A at ESRF/DUBBLE (Grenoble, France). These spectra were collected in the fluorescence mode in a 90° orientation to the incident X-ray beam, by using a nine-channel monolithic germanium detector. A Si(111) monochromator crystal was used. In the first series of experiments the samples were pressed into self-supporting wafers and placed in a controlled atmosphere cell, which was flushed with He at room temperature prior to measurement. Each spectrum was collected over a 45 min period, at 77 K, and several scans were recorded for averaging (to be able to improve the signal to noise ratio of the data). In a second series of experiments the same samples were measured in air at room temperature. The XAFS data were processed using the programmes available at Daresbury laboratory, that is, EXCALIB (for converting the raw data to energy vs. absorption coefficient) and EXBROOK (for pre and post-edge background removal) to obtain the normalized XANES part of the spectra and EXCURV98[16] in order to carry out EXAFS data analysis. EXAFS refinements were carried out on k^3-weighted spectra plotted over a k range of 3–13.3 $Å^{-1}$ considering only single scattering paths. An amplitude reduction factor (S_o^2) value of 0.9, obtained from fitting a Cu metal foil, was also used in the analysis. Since the Cu–O and Cu–N bond lengths and backscattering amplitudes are of the same order, it is difficult to distinguish between their respective contributions in EXAFS. This is a particular problem for the Cu^{2+}/His system, in which the two different atoms, O and N, are coordinating in the same coordination shell. As the fitting of two shells with the respective atoms resulted in unphysical results, the refinements were performed considering only a single shell of either Cu–O or Cu–N with the best fit of the data being determined by the R factor.

IR spectra were recorded at room temperature on a Perkin–Elmer 2000 FTIR spectrometer with a DTGS detector. Samples were prepared as KBr pellets and for each spectrum 256 scans were accumulated at a data point resolution of 2 cm^{-1} (optical resolution 4 cm^{-1}). The spectrum of dried air was used as background.

Raman measurements were carried out on a Perkin–Elmer 2000 FT-Raman system equipped with an InGaAs detector and a 1064 nm NdYag laser for excitation. Scanning was performed in back scattering mode at a laser output power of 100 mW and a data point resolution of 4 cm^{-1} (optical resolution 8 cm^{-1}). For each spectrum 500 scans were accumulated. Spectral subtraction procedures were applied for both IR and Raman in order to compensate for bands of the support material.

Acknowledgements

John Raaymakers[1r] and Ad Mens are kindly acknowledged for the N_2 physisorption measurements and Ad van der Eerden for the XRF analysis. Robert Schoonheydt is thanked for supplying the ESR facilities in Leuven and Ernst van Faassen for the assistance in the interpretation of the ESR results. The European Synchrotron Radiation Facility (ESRF, Grenoble, France) and Hasylab (Hamburg, Germany) are acknowledged for the provision of synchrotron radiation facilities. We thank M. Borowski (BM29) and W. Bras and S. Nikitenko of DUBBLE (BM26A, ESRF) for their help and discussion during the experiments. NWO-CW, van der Leeuw and the National Research School Combination, and Catalysis (NRSC-C) are acknowledged for financial support.

[1] R. J. Sundberg, R. B. Martin, *Chem. Rev.* **1974**, *74*, 471–517.
[2] *Handbook on Metalloproteins* (Eds.: I. Bertini, A. Sigel, H. Sigel), Marcel Dekker, New York, **2001**.
[3] *Bioinorganic Catalysis* (Eds.: J. Reedijk, E. Bouwman), Marcel Dekker, New York, **1999**.
[4] K. Buchholz, V. Kasche, U. T. Bornscheuer, *Biocatalysts and Enzyme Technology*, Wiley-VCH, Weinheim, **2005**.
[5] *Artificial Enzymes* (Ed.: R. Breslow), Wiley-VCH, Weinheim, **2005**.
[6] A. S. Bommarius, B. R. Riebel, *Biocatalysis*, Wiley-VCH, Weinheim, **2004**.
[7] B. M. Weckhuysen, A. A. Verberckmoes, I. P. Vannijvel, J. A. Pelgrims, P. L. Buskens, P. A. Jacobs R. A. Schoonheydt, *Angew. Chem.* **1995**, *107*, 2868–2870; *Angew. Chem. Int. Ed. Engl.* **1995**, *34*, 2652–2654.
[8] D. Baute, D. Arieli, F. Neesse, H. Zimmermann, B. M. Weckhuysen, D. Goldfarb, *J. Am. Chem. Soc.* **2004**, *126*, 11733–11745.
[9] D. E. deVos, P. P. Knops-Gerrits, R. F. Parton, B. M. Weckhuysen, P. A. Jacobs, R. A. Schoonheydt, *J. Inclusion Phenom. Mol. Recognit. Chem.* **1995**, *21*, 185–213.
[10] L. Fu, B. M. Weckhuysen, A. A. Verberckmoes, R. A. Schoonheydt, *Clay Miner.* **1996**, *31*, 491–500.
[11] R. Grommen, P. Manikandan, Y. Gao, T. Shane, J. J. Shane, R. A. Schoonheydt, B. M. Weckhuysen, D. Goldfarb, *J. Am. Chem. Soc.* **2000**, *122*, 11488–11496.
[12] B. M. Weckhuysen, A. A. Verberckmoes, L. Fu, R. A. Schoonheydt, *J. Phys. Chem.* **1996**, *100*, 9456–9461.
[13] P. Comba, *Coord. Chem. Rev.* **2000**, *200–202*, 217–245.
[14] J. G. Mesu, T. Visser, F. Soulimani, B. M. Weckhuysen, *Vib. Spectrosc.* **2005**, *39*, 114–125.
[15] J. G. Mesu, T. Visser, F. Soulimani, E. E. van Faassen, P. de Peinder, A. M. Beale, B. M. Weckhuysen, *Inorg. Chem.* **2006**, *45*, 1960–1971.
[16] N. Binsted, J. W. Campbell, S. J. Gurman, P. C. Stephenson, *EXAFS Analysis Programs*, Daresbury Laboratory, Warrington, **1991**.
[17] R. W. Strange, L. Alagna, P. Durham, S. S. Hasnain, *J. Am. Chem. Soc.* **1990**, *112*, 4265–4288, and references therein.
[18] C. Lamberti, G. Spoto, D. Scarano, C. Pazé, M. Salavaggio, S. Bordiga, A. Zecchina, G. Turnes Palomino, F. D'Acapito, *Chem. Phys. Lett.* **1997**, *269*, 500–508.
[19] L. Kau, D. Spira-Solomon, J. E. Penner-Hahn, K. Hodgson, E. I. Solomon, *J. Am. Chem. Soc.* **1987**, *109*, 6433–6442.
[20] J. Garcia, M. Benfatto, C. R. Natoli, A. Bianconi, A. Fontaine, H. Tolentino, *Chem. Phys.* **1989**, *132*, 295–302.
[21] J. Chaboy, A. Muňoz-Páez, F. Carrera, P. Merkling, E. Sánchez Marcos, *Phys. Rev. B* **2005**, *71*, 134208.
[22] J. G. Mesu, A. M. J. van der Eerden, F. M. F. de Groot, B. M. Weckhuysen, *J. Phys. Chem. B* **2005**, *109*, 4042–4047.
[23] A. B. P. Lever, *Inorganic Electronic Spectroscopy*, Elsevier Science BV, Amsterdam, **1984**.
[24] E. W. Wilson, M. H. Kasperian, R. B. Martin, *J. Am. Chem. Soc.* **1970**, *92*, 5365–5372.
[25] E. Bernarducci, W. F. Schwindinger, J. L. Hughey, K. Krogh-Jespersen, H. J. Schugar, *J. Am. Chem. Soc.* **1981**, *103*, 1668–1675.
[26] E. Bernarducci, P. K. Bharadwaj, K. Krogh-Jespersen, H. J. Schugar, *J. Am. Chem. Soc.* **1983**, *105*, 3860–3866.
[27] T. G. Fawcett, E. E. Bernarducci, K. Krogh-Jespersen, H. J. Schugar, *J. Am. Chem. Soc.* **1980**, *102*, 2598–2604.

Received: January 19, 2006
Published online: June 29, 2006

